PCCP

Molecular Dynamics Simulations of Alkaline Earth Metal Ions Binding to DNA Reveal Ion Size and Hydration Effects

Journal:	*Physical Chemistry Chemical Physics*
Manuscript ID	CP-ART-12-2019-006844.R1
Article Type:	Paper
Date Submitted by the Author:	07-Feb-2020
Complete List of Authors:	Long, Makenzie; University of Central Arkansas, Chemistry Alland, Serra; University of Central Arkansas, Chemistry Martin, Madison; University of Central Arkansas, Chemistry Isborn, Christine; University of California Merced, Chemistry and Chemical Biology

SCHOLARONE™
Manuscripts

Molecular Dynamics Simulations of Alkaline Earth Metal Ions Binding to DNA Reveal Ion Size and Hydration Effects

Makenzie Provorse Long,*[a] Serra Alland, [a] Madison E. Martin,[a] and Christine M. Isborn [b]

The identity of metal ions surrounding DNA is key to its biological function and material applications. In this work, we compare atomistic molecular dynamics simulations of double strand DNA (dsDNA) with four alkaline earth metal ions (Mg^{2+}, Ca^{2+}, Sr^{2+}, and Ba^{2+}) to elucidate the physical interactions that govern DNA-ion binding. Simulations accurately model the ion-phosphate distance of Mg^{2+} and reproduce ion counting experiments for Ca^{2+}, Sr^{2+}, and Ba^{2+}. Our analysis shows that alkaline earth metal ions prefer to bind at the phosphate backbone compared to the major groove and negligible binding occurs in the minor groove. Larger alkaline earth metal ions with variable first solvation shells (Ca^{2+}, Sr^{2+}, and Ba^{2+}) show both direct and indirect binding, where indirect binding increases with ion size. Mg^{2+} does not fit this trend because the strength of its first solvation shell predicts indirect binding only. Ions bound to the phosphate backbone form fewer contacts per ion compared to the major groove. Within the major groove, metal ions preferentially bind to guanine-cystosine base pairs and form simultaneous contacts with the N7 and O6 atoms of guanine. Overall, we find that the interplay among ion size, DNA-ion interaction, and the size and flexibility of the first solvation shell are key to predicting how alkaline earth metal ions interact with DNA.

Introduction

Metal ions play an important role in the structure and function of nucleic acids, including DNA replication and efficient DNA packing.[1–3] In addition to its biological importance, the structural, electronic, and optical properties of DNA make it a robust and versatile material in nanoscale devices.[4–11] DNA-based nanotechnology includes electric and optoelectric devices,[12–16] drug delivery and therapeutics,[17–19] sensing,[10,20–28] and imaging.[29,30] These applications often rely on divalent metal ions to stabilize the structure of DNA, induce aggregation or adsorption, bind substrates, quench or enhance spectroscopic signals, or alter the electric or optoelectric properties of DNA. The identity of the metal ion affects the structural, electronic, optical, and chemical properties of DNA;[12,16,19,20,22,27] however, an atomistic understanding of how DNA-ion interactions vary for different metal ions is lacking. A thorough understanding of the physical characteristics that govern the interactions between DNA and metal ions, such as binding site preference and binding motif, will provide insight that can be manipulated for future nanotechnological applications.

The alkaline earth metal ions Mg^{2+}, Ca^{2+}, Sr^{2+}, and Ba^{2+} offer a unique opportunity to investigate the effects of ion size and hydration behavior of divalent metal ions on DNA-ion binding, without being complicated by open-shell electronic structure.

These ions have a closed-shell electronic structure and predictable changes in hydration behavior. The experimental first solvation shell coordination number of Mg^{2+} is typically 6.0[31,32] and the coordination numbers of Ca^{2+}, Sr^{2+}, and Ba^{2+} are 8.0, 8.0-9.0, and 9.0-9.5, respectively.[31,33–38] The experimental residence time of water molecules within the first solvation shell of Mg^{2+} is 10^{-6} s,[39,40] whereas Ca^{2+}, Sr^{2+}, and Ba^{2+} have shorter residence times of 10^{-8} to 10^{-10} s.[41] Thus, the size and flexibility of the first solvation shell of alkaline earth metal ions increases as the ionic radius increases. However, as the ionic radius increases, the DNA-ion electrostatic interaction is expected to decrease due to Coulomb's law. These electronic and hydration effects likely determine how alkaline earth metal ions bind to DNA.

Experimental and theoretical studies show that alkaline earth metal ions tend to localize near the negatively charged phosphate backbone of double-strand DNA (dsDNA), forming an ion atmosphere or sheath.[42–47] Buffer equilibration and atomic emission spectroscopy studies show that the relative affinity of alkaline earth metal ions for the dsDNA ion atmosphere is $Ca^{2+} \approx Mg^{2+} > Sr^{2+} \geq Br^{2+}$, which inversely correlates with the size of the solvated ion.[46] This trend is independent of the DNA sequence and length, which suggests that alkaline earth metal ions do not bind to specific atomic sites.[46] Other experimental studies suggest that alkaline earth metals Mg^{2+} and Ca^{2+} bind to guanine within the major groove of dsDNA,[45,48] but they have a larger preference for the phosphate backbone compared to transition metal ions.[47] In general, alkaline earth metal ions preferentially bind to the phosphate backbone of dsDNA and this preference correlates with solvated ion size.

a. Department of Chemistry and Biochemistry, University of Central Arkansas, Conway, Arkansas 72035, United States. E-mail: mlong14@uca.edu
b. Chemistry and Chemical Biology, University of California Merced, Merced California 95343, United States.

In addition to binding site preference, another aspect of characterizing DNA-ion interactions is distinguishing between direct and indirect binding motifs. Indirect binding occurs when the first solvation shell of a metal ion remains intact and one or more hydrogen bonds are formed between the water molecules of the first solvation shell and DNA. Direct binding occurs when a direct interaction between the metal ion and DNA is formed. Experimental studies provide conflicting results: some studies indicate that alkaline earth metal ions Mg^{2+} and Ca^{2+} prefer indirect binding,[43–52] but others show evidence of direct binding[43,48,51,53,54] and simultaneous direct and indirect binding.[51,54,55] Due to their size, Ca^{2+} and Ba^{2+} can form more than one direct contact to DNA.[54] A quantitative analysis of the probability of binding motifs will provide additional insight into the physical interactions that govern DNA-ion interactions.

Atomistic molecular dynamics simulations provide statistically relevant information about DNA-ion interactions. Alkaline earth metal ions are expected to bind to dsDNA through electrostatic and van der Waals interactions due to their closed-shell electronic structure; therefore, classical force fields can accurately model DNA-ion interactions of alkaline earth metal ions. In fact, there are many studies that use molecular dynamics simulations to model the interactions of Mg^{2+} ions with DNA,[56–60] due to its biological relevance and readily available force field parameters.[61–63] In agreement with experimental evidence, Mg^{2+} displaces monovalent cations near dsDNA and primarily binds to the phosphate backbone and the major groove through indirect binding.[56–59] Within the major groove, Mg^{2+} preferentially binds to guanine-cytosine (GC) base pairs rather than adenine-thymine (AT) base pairs. This sequence-specific binding of Mg^{2+} is attributed to electronic rather than steric effects and is mediated by the first solvation shell of Mg^{2+}.[56] However, the Mg^{2+}-phosphate interaction is overestimated by many force fields, which can be addressed by reparameterization or alternative force field models.[61,64,65]

Other computational approaches use more complex molecular dynamics simulations[64–73] or small-molecule quantum mechanical calculations[45,74,83,75–82] to model DNA-ion interactions. These approaches, however, are limited to the metals for which the methods have been developed or are restricted to geometries optimized at 0 K, which may not be statistically relevant at physiological and experimental temperatures. Atomistic molecular dynamics simulations using validated classical force fields have the ability to provide a detailed molecular view of statistically relevant structures of dsDNA solvated by different alkaline earth metal ions.

In this work, atomistic molecular dynamics simulations are used to sample structures of a 23-mer DNA duplex in aqueous solution with Mg^{2+}, Ca^{2+}, Sr^{2+}, or Ba^{2+} ions (Fig. 1). The alkaline earth metal ions are treated on equal footing using force field parameters[84] optimized by Merz and co-workers to reproduce experimental hydration free energies, ion-water distances, and coordination numbers. These parameters are validated by comparing simulation results to experimental DNA-ion binding data, including experimental ion-phosphate distances and ion counting experiments. For the first time, the preferred bindings sites and binding motifs of these alkaline earth metal ions with

dsDNA are quantified and compared. This work reveals that the size and flexibility of the first solvation shell of metal ions are important factors to determine DNA-ion binding trends.
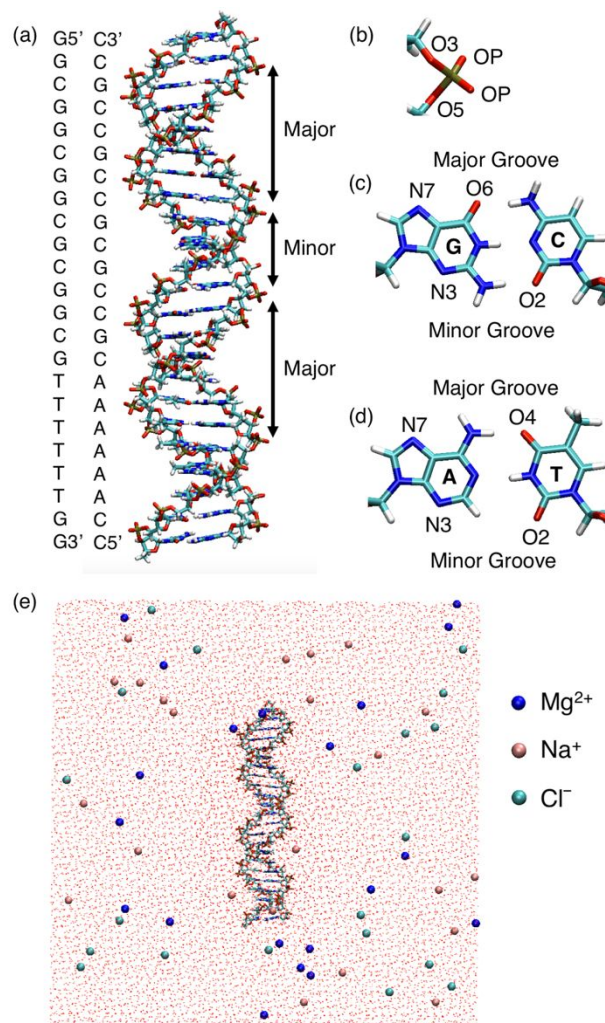

Fig. 1 (a) Nucleotide sequence and molecular structure of the 23-mer DNA duplex. Double headed arrows signify the major and minor grooves. Molecular structure of the (b) phosphate group and the (c) guanine (G) – cysteine (C) and (d) adenine (A) – thymine (T) base pairs. Labels show the electronegative atoms on the phosphate backbone and major and minor grooves. (d) Initial configuration of dsDNA, ions, and water oxygen atoms in the simulation box.

Computational Details

Molecular Simulations

Atomistic molecular dynamics simulations were performed using the GROMACS program version 5.0.7.[85] A 23-mer DNA duplex (Fig. 1a) with a nucleotide sequence of 5'-GGCGGCGGCGCGGCGTTTTTTGG-3' was solvated in a 150 Å x 150 Å x 150 Å cubic box of water molecules with 20 divalent metal ions (Mg^{2+}, Ca^{2+}, Sr^{2+}, or Ba^{2+}), 24 Na^+ ions, and 20 Cl^- ions (Fig. 1e). This DNA duplex was chosen because previous molecular dynamics simulations of this sequence demonstrated that the GC track preferentially bound Mg^{2+} ions compared to the AT track,[56] which offers an interesting comparison for other alkaline earth metal ions studied here. The concentration of divalent ions in each simulation was ~10 mM and the total salt

concentration was ~20 mM. The bulk concentration of divalent ions at large distances from the DNA duplex was ~5 mM. This bulk concentration was calculated using a procedure similar to Yoo and Aksimentiev,[57] which is described in detail in the electronic supporting information (ESI). The explicit water molecules were described by the TIP3P water model.[86] DNA was modeled by the AMBER99SB force field with ParmBSC0 nucleic acid torsions.[87,88] Although refined DNA force fields, such as BSC0$_{OL15}$[89] and BSC1,[90] improve the structural model of the DNA helix, especially in preventing fraying at the ends of the helix,[91] these force fields were not available at the beginning of this project. For consistency, we used BSC0 for all simulations presented here, which provides a reasonable model of the DNA helix.[91] The Na$^+$ and Cl$^-$ ions were modeled by the Lennard-Jones parameters optimized by Åqvist.[62] The alkaline earth metal ions were modeled by the Lennard-Jones parameters optimized by Merz and co-workers to reproduce the relative experimental hydration free energies, coordination numbers, and distances between the ion and oxygen atom of water molecules in the first solvation shell of each ion for a set of 24 divalent metal ions, called the 'compromise' set of parameters (Table S1).[84] Although other classical force field approaches[64,65,72,73] are available for most metal ions studied here, a direct comparison of the performance of these approaches is not the focus of this work.

All energy minimization, equilibration, and production simulations were run using a van der Waals cutoff of 10 Å (to match that used in the optimization of the divalent metal ion Lennard-Jones parameter simulations) and particle mesh Ewald summation[92] with a cutoff of 10 Å and a grid spacing of 1.2 Å. The non-bonded list was updated every 10 steps with a cutoff of 10 Å. All equilibration and production simulations used the velocity rescaling thermostat[93] and Parrinello-Rahman barostat[94] to simulate an NPT ensemble at 1 bar and 300 K. A time integration step of 2 fs was used with all water hydrogen bonds constrained by the SETTLE algorithm.[95] Each simulation was equilibrated for 10 ps with all DNA bonds constrained by the P-LINCS algorithm[96] followed by 100 ps of equilibration with only the DNA hydrogen bonds constrained. A 500 ns (Mg^{2+}, Sr^{2+}, and Ba^{2+}) or 800 ns (Ca^{2+}) production simulation was then run using the P-LINCS algorithm[96] to constrain the DNA hydrogen bonds.

Equilibration and production simulations were started from the same set of atomic coordinates to avoid dependence on the initial placement of ions. These initial coordinates were generated from a series of energy minimization steps. The DNA duplex was minimized in vacuum using 5000 steepest descent energy minimization steps. The genbox tool of GROMACS was then used to surround the minimized DNA structure with more than 117,200 pre-equilibrated TIP3P water molecules, followed by another 5000 steepest descent energy minimization steps. The genion GROMACS tool was then used to replace water molecules with 20 Mg^{2+}, 24 Na$^+$ ions, and 20 Cl$^-$ ions, leaving a total of 117,185 water molecules. Of the 20 Mg^{2+} ions added, 19 were placed at least 15 Å from the nearest DNA atom and 1 was placed ~8 Å from the nearest DNA atom. This structure was minimized using 5000 steepest descent energy minimization

steps, where the divalent ions were modeled using the Lennard-Jones parameters of Mg^{2+} optimized by Li et al.[84] This minimized structure, which resulted in fully hydrated Mg^{2+} ions, was used as the initial coordinates for equilibration and production simulations for each alkaline earth metal ion (Mg^{2+}, Ca^{2+}, Sr^{2+}, or Ba^{2+}).

The convergence of each production simulation was evaluated by the fluctuation in the average number of divalent ions bound to DNA computed using 50 ns intervals (Fig. S1). The Ca^{2+} simulation has a large increase in the number of divalent ions bound to DNA within the first 100 ns. To verify this is not an artifact of initial positions of the divalent ions, a second Ca^{2+} simulation was run using different initial coordinates, where the divalent ions were placed at least 10 Å from any DNA atom. This second simulation predicts a similar number of bound ions as the original Ca^{2+} simulation (Fig. S1). For all DNA-ion simulations, the average number of divalent ions bound to DNA between 100 ns and 200 ns fluctuates by less than 1 ion relative to the average value computed for the last 450 ns (Mg^{2+}, Sr^{2+}, and Ba^{2+}) or 750 ns (Ca^{2+}) of each production simulation (Table S2). Therefore, further analysis was performed on the 100 ns to 200 ns section of each production simulation.

The experimental residence time of water molecules within the first solvation shell Mg^{2+} is larger (~1 μs)[39,40] than the length of the production simulations; therefore the simulations presented here do not sample water exchange for Mg^{2+} ions. However, the water residence time for Ca^{2+}, Sr^{2+}, and Ba^{2+} is relatively short (~10 ns)[41] and simulations presented in this work accurately model water exchange for these ions. Ion pairing is not observed within the first 500 ns of the Mg^{2+} and Ca^{2+} production simulations (Fig. S2). Although 500 ns is less than the Mg^{2+} water residence times, it is sufficiently longer than the Ca^{2+} water residence times; thus, these simulations are converged with respect to ion pairing.

Analysis

The spatial distribution of ions surrounding DNA was analyzed using radial distribution functions (RDFs) and occupancy of DNA binding sites. Because terminal base pairs may separate during simulation, two terminal base pairs on either end of the DNA duplex were omitted from analysis. RDFs and coordination numbers (computed from the integration of an RDF) were calculated using the rdf tool of GROMACS. The relative height of an RDF indicates the probability of an atom at that radial distance. However, the non-spherical shape of DNA distorts the normalization procedure and overestimates peak heights at small radial distances.[97] Therefore, occupancy is used for quantitative analysis rather than integration of RDFs. Occupancy is defined as the ratio of the number of ions bound to dsDNA relative to the total number of ions present in the simulation. Occupancy is averaged over the number of frames analyzed. Here, occupancy values were calculated from 20 frames spaced 5 ns apart and standard deviations were calculated from these time averages. To test the convergence of these results with respect to sampling, occupancy values were calculated for Sr^{2+} and Ba^{2+} using 100 frames selected 1 ns apart, which gave similar results (Table S3).

A bound ion is typically defined using a distance cutoff, where ions within a given distance from DNA are considered bound. Previous molecular dynamics simulation studies of Mg^{2+} ions with a DNA duplex use a distance cutoff of 5 or 6 Å.[56,57] Here the cutoff distance is defined as the minimum distance that includes the water oxygen atoms within first and second solvation shells of the metal ion. This approach includes ions both directly and indirectly bound to DNA. The number of bound ions defined by a distance cutoff was calculated using the mindist tool of GROMACS. The group option was used to define multiple contacts between an ion and several DNA atoms as one bound ion. We also applied an alternative approach for calculating the number of bound ions using a distance cutoff equal to the first solvation shell to define direct binding and a distance cutoff equal to the second solvation shell and a secondary requirement that an oxygen atom of the water molecules within the first solvation shell are within 2.5 Å of the DNA atom to define indirect binding. By verifying that a water molecule within the first solvation shell of the ion is within hydrogen bonding distance of the DNA atom, this approach accurately identifies Ca^{2+}, Sr^{2+}, and Ba^{2+} ions indirectly bound to DNA atoms due to the variable first solvation shells of these ions.

The DNA-ion residence time was calculated as the length of time a single ion is continuously bound to DNA using snapshots saved every 10 ps from 100 ns to 200 ns of each production simulation. Each instance of an ion binding and unbinding is called a binding event. The total number of binding events for each divalent metal ion is binned according to the length of the binding event (i.e., the residence time). The distribution of residence times for each divalent metal ion is reported as a percentage of the total number of binding events for that ion.

Additional Simulations

The simulations presented in this work do not predict direct binding between Mg^{2+} and dsDNA. Additional simulations were performed to investigate direct binding of Mg^{2+} ions at the phosphate backbone and major groove of dsDNA. In general, Mg^{2+} ions remain directly bound to the phosphate backbone once a direct contact has formed. Within the major groove, multiple direct binding events are not observed for Mg^{2+} (i.e., once a direct contact is lost, the ion does not reform a direct contact). Additional information about these direct binding simulations are provided in the ESI.

Simulations of transition metal ions (Ni^{2+} and Co^{2+}) binding to dsDNA were performed using the same simulation protocols as the alkaline earth metal ion simulations. These ions behave similarly as Mg^{2+} due to their tightly held first solvation shell with hexa-coordinated water molecules. However, the classical force field[84] used here significantly underestimates the ion-phosphate distance for these transition metal ions. Therefore, the transition metal ion simulations are not reliable. The force field used does not account for charge transfer or covalent bonds, which may be important for accurately modeling transition metal ion interactions with dsDNA, but it accurately models metal ion hydration. Additional results from these transition metal ions simulations are provided in the ESI.

Results and Discussion

Validation of Alkaline Earth Metal Ion Force Field

The force field parameters used in this study to model alkaline earth metal ions were optimized to reproduce experimental hydration data.[84] It is unclear how transferable these ion parameters are for modeling DNA-ion interactions. To verify these parameters accurately model DNA-ion interactions, we first compare simulation results to previously reported experimental and computational results.

Simulations herein reproduce the size-dependent trends of Ca^{2+}, Sr^{2+}, and Ba^{2+} ions reported by ion counting experiments (Table S4).[46,98] Despite the fact that our simulations use slightly different background ion concentrations (e.g., 10 mM versus 20 mM Na^+), they reproduce the experimental number of excess divalent ions within experimental and simulation error. All divalent metal ions studied here displace monovalent cations (Na^+) near dsDNA (Fig. S3), in agreement with experimental studies[46,99,100] and previous simulations of Mg^{2+} with dsDNA.[56,57] In addition, the incorrect ion pair formation of Cl^- ions and Ca^{2+} ions bound to dsDNA predicted by previous simulations[72] is not observed in the current work (Fig. S2). However, the number of excess Mg^{2+} ions bound to dsDNA is underestimated relative to an ion counting experiment,[46] which may be due to a lack of direct binding predicted by the current force field.

Another experimental observable used to validate force fields for DNA-ion simulations is the ion-phosphate distance. The Mg^{2+} parameters developed by Li et al.[84] used herein improve or reproduce Mg^{2+}-phosphate distances reported by previous simulations[61] and are physically reasonable relative to a known experimental value[101] (Table S5). These results are in contrast to previous simulations in which ion-phosphate and ion-carboxylate interactions are overestimated.[61,64,65,72,102–105]

In summary, the alkaline earth metal ion force field parameters used here capture valid ion-DNA interactions as shown by comparison with ion counting experiments and ion-phosphate distances. In addition, unphysical ion pair formation is not observed and all divalent ions displace monovalent ions near DNA. Together, these results demonstrate the force field developed by Li et al.[84] is appropriate for modeling DNA-ion interactions of alkaline earth metal ions.

Alkaline Earth Metal Ion Solvation

The structure of the first solvation shell of a metal ion influences its ability to bind directly versus indirectly to DNA. RDFs provide statistically-averaged information about the size and number of water molecules in the solvation shell of each ion. The RDFs between each alkaline earth metal ion and water oxygen atoms in the presence of dsDNA are shown in Fig. 2. The first peak of the Mg^{2+} RDF is relatively tall and narrow, indicating that this ion has a well-defined first solvation shell. Water oxygen atoms in the first solvation shell are located 1.8-2.3 Å from the ions, consistent with experimental ion-oxygen distances of 2.0-2.2 Å.[31] The second peak of the Mg^{2+} RDF illustrates that the water oxygen atoms within the second solvation shell are located 3.5-5.0 Å from the ion. The first peaks of the Ca^{2+}, Sr^{2+}, and Ba^{2+} RDFs are shorter and wider than that of Mg^{2+}, indicating the first

ARTICLE

solvation shells of Ca^{2+}, Sr^{2+}, and Ba^{2+} are more varied in the number of water molecules within the shell and the ion-water oxygen distances. The water oxygen atoms within the first solvation shells of Ca^{2+}, Sr^{2+}, and Ba^{2+} are located 2.3-3.4 Å from the ions. The most probable ion-water oxygen distance increases as the ionic radius increases: 2.5 Å, 2.7 Å, and 2.9 Å for Ca^{2+}, Sr^{2+}, and Ba^{2+}, respectively, consistent with experiment.[31] A similar trend is observed for the second solvation shells of Ca^{2+}, Sr^{2+}, and Ba^{2+} with water oxygen atoms located 3.9-6.2 Å from the ions. In the following discussion, the radial distances of the first and second solvation shells for each ion are used to identify direct and indirect binding to DNA, respectively.
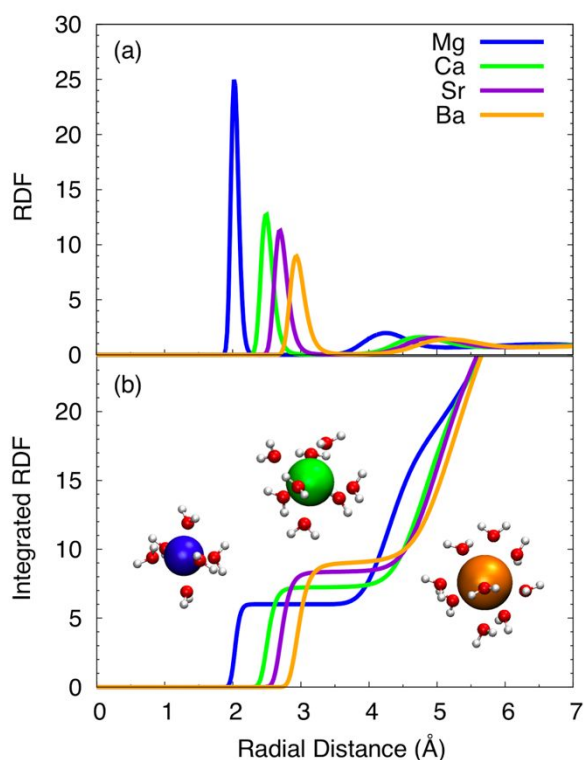

Fig. 2 (a) RDF and (b) integrated RDF between each alkaline earth metal ion and water oxygen atoms. Insets show Mg^{2+} (blue), Ca^{2+} (green), and Ba^{2+} (orange) solvated by 6, 8, and 9 water molecules, respectively. Ions are shown with unscaled van der Waals radii.

The value of an integrated RDF at an inflection point gives the coordination number of the central atom. Based on its integrated RDF (Fig. 2b), Mg^{2+} has a coordination number of 6.0. Therefore, Mg^{2+} maintains 6 water molecules in its first solvation shell throughout the simulation and is expected to interact with dsDNA through indirect binding only, in agreement with experiment[43–52] and previous molecular dynamics simulations.[56,58–60] Although not predicted by the simulation methods used here, direct binding between Mg^{2+} and DNA has been reported experimentally.[43,48,51,54] Alternative force field parameterization or different atomistic models may be necessary to simulate this binding motif.

The integrated RDFs (Fig. 2b) show that Ca^{2+}, Sr^{2+}, and Ba^{2+} have coordination numbers of 7.3, 8.6, and 9.3, respectively. The first solvation shells of Ca^{2+}, Sr^{2+}, and Ba^{2+} are flexible (i.e.,

non-integer values) and increase with ionic radius, in agreement with experiment.[31,33–38] Due to the flexibility of the first solvation shells of these ions, the simulation methods used here predict both direct and indirect binding of Ca^{2+}, Sr^{2+}, and Ba^{2+} to dsDNA.

DNA Binding Sites

Metal ions may bind to three areas of dsDNA: the phosphate backbone, the major groove, and the minor groove (Fig. 1). Both steric and electronic effects play a role in determining where solvated metal ions bind to dsDNA. To identify preferred DNA binding sites, we analyze RDFs of each metal ion within each DNA binding site.

Phosphate Backbone. The RDFs between each alkaline earth metal ion and the oxygen atoms of the phosphate backbone (Fig. 1b) are shown in Fig. 3. Note that due to the asymmetrical shape of dsDNA, the normalization procedure overestimates RDF peak heights near DNA (i.e., small radial distances); however, the location of RDF peaks accurately reflects the location of ions relative to dsDNA, which we focus on here. The first peaks of the Ca^{2+}, Sr^{2+}, and Ba^{2+} RDFs are located with the first solvation shells of these ions, indicating direct as well as indirect binding. In contrast, the first peak of the Mg^{2+} RDF is located within the second solvation shell of Mg^{2+}. Therefore, Mg^{2+} indirectly binds to the phosphate backbone, whereas Ca^{2+}, Sr^{2+}, and Ba^{2+} may directly or indirectly bind to the phosphate backbone.
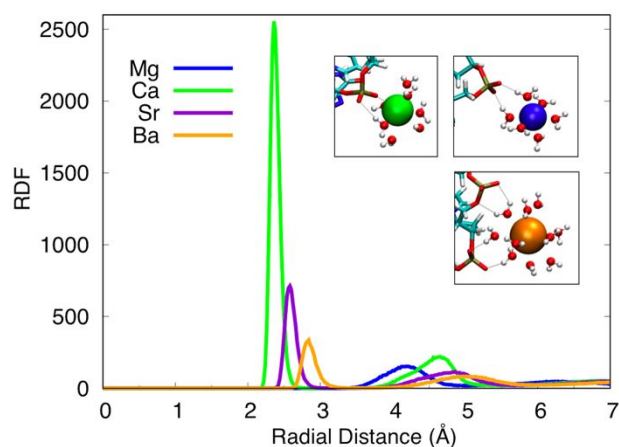

Fig. 3 The RDF between each alkaline earth metal ion and the oxygen atoms of the phosphate backbone of dsDNA. Insets show Ca^{2+} (green) directly bound to a phosphate group and Mg^{2+} (blue) and Ba^{2+} (orange) indirectly bound to one or two phosphate groups, respectively. Ions are shown with unscaled van der Waals radii.

Additional analysis (Fig. S4) suggests that the majority of metal ions indirectly bound to the phosphate backbone of dsDNA form one or two hydrogen bonds to the same phosphate group and a small portion form three or more hydrogen bonds to phosphate groups next to one another along the same DNA strand, called neighboring residues. Negligible binding occurs between phosphate groups on opposite DNA strands, regardless of ionic radius or the size and flexibility of the first solvation shell of the ion (Fig. S4). For metal ions that directly bind to the phosphate backbone (Ca^{2+}, Sr^{2+}, and Ba^{2+}), the

majority of bound ions form one direct contact only or one direct contact and one or two indirect contacts on the same or neighboring phosphate residues as the direct contact (Fig. S5). In general, alkaline earth metal ions bound to the phosphate backbone of dsDNA form one or two contacts to the same or neighboring phosphate groups, regardless of the binding motif (i.e., direct or indirect) and binding across DNA strands is rarely observed.

Minor Groove. The RDFs between each divalent metal ion and the electronegative atoms of the minor groove (N3 of adenine, O2 of thymine, N3 of guanine, and O2 of cytosine) are shown in Fig. S6. The peaks are relatively small, which suggest negligible binding to the minor groove, in agreement with experiment and previous molecular dynamics simulations.[56–59] There are no peaks within the first solvation shell of any divalent ion; therefore, if a divalent ion is present in the minor groove, it is indirectly bound. Previous work indicates that steric effects are responsible for negligible binding of Mg^{2+} in the minor groove of dsDNA,[56] which is likely the case for the other alkaline earth metal ions studied here.

Major Groove. The RDF peaks for the N7 and O6 atoms of guanine are significantly larger than those of adenine N7 and thymine O4 (Fig. S7), making the guanine N7 and O6 atoms the preferred binding sites of alkaline earth metal ions within the major groove of dsDNA. Additional analysis suggests that binding to adenine N7 or thymine O4 is likely due to strong interactions with N7 and O6 atoms of neighboring guanine residues or nearby phosphate oxygen atoms (Fig. S7).

indirectly bound to neighboring guanine residues with simultaneous hydrogen bonds to the N7 and O6 atoms. Ions are shown with unscaled van der Waals radii.

The RDFs between each alkaline earth metal ion and the N7 and O6 atoms of guanine within the major groove of dsDNA are shown in Fig. 4. Ba^{2+} and Sr^{2+} may be directly or indirectly bound to the major groove at the N7 and O6 atoms of guanine, whereas Ca^{2+} predominately binds through indirect contacts. Mg^{2+} ions are indirectly bound only. Additional analysis reveals that the majority of metal ions bound to the major groove of dsDNA form three or more hydrogen bonds to neighboring residues along the same DNA strand or neighboring residues and their respective base pairs on the opposite DNA strand (Fig. S8). In general, the N7 and O6 atoms of guanine are the preferred binding sites within the major groove of dsDNA and alkaline earth metal ions bound to these sites form more contacts per ion compared to ions bound to the phosphate backbone.

Quantitative Analysis of DNA-Ion Binding

To quantify the probability of each alkaline earth metal ion binding to a specific DNA binding site, the occupancy is computed for each ion. Occupancy is the ratio of the average number of bound ions compared to the total number of ions in the simulation. An ion is considered bound when dsDNA is within a radial distance that defines the first or second solvation shell of the ion (Fig. 2a). Occupancy is a time-averaged quantity that reflects the average distribution of alkaline earth metal ions bound to dsDNA throughout the length of each simulation.
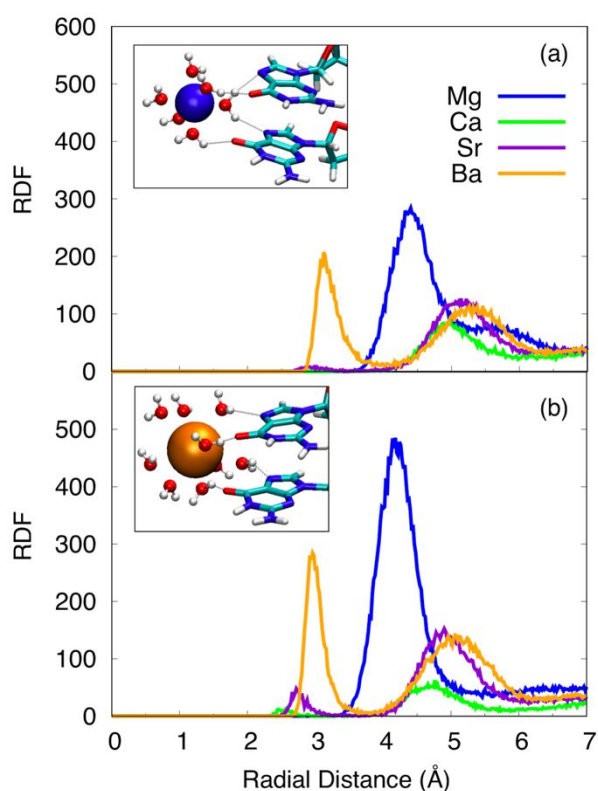

Fig. 4 The RDFs between each alkaline earth metal ion and the (a) N7 and (b) O6 atoms of guanine in the major groove of dsDNA. Insets show Mg^{2+} (blue) and Ba^{2+} (orange)
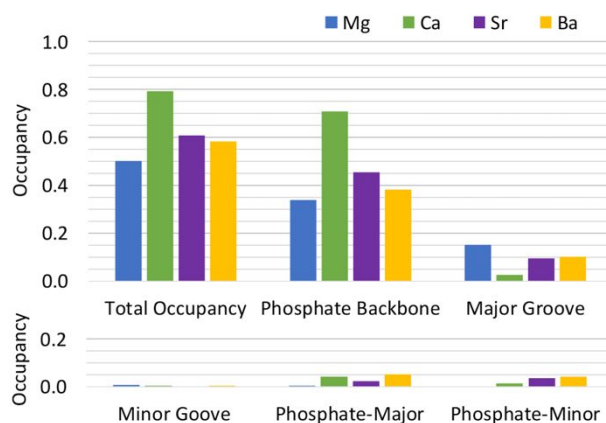

Fig. 5 Occupancy of DNA binding sites by alkaline earth metal ions.

The occupancy of each DNA binding site and the total occupancy are shown in Fig. 5. Occupancy values with time-average standard deviations are provided in Table S6. The total occupancy is the sum of the occupancy of all five DNA binding sites (phosphate backbone, major groove, minor groove, and simultaneous binding to the phosphate backbone and the major or minor groove). Total occupancy of DNA ranges from 0.50 to 0.79 and decreases in the following order: $Ca^{2+} > Sr^{2+} > Ba^{2+} > Mg^{2+}$. The total occupancy of DNA by Ca^{2+}, Sr^{2+}, and Ba^{2+} agrees with the experimental preference of these ions for the DNA ion atmosphere ($Mg^{2+} \sim Ca^{2+} > Sr^{2+} > Ba^{2+}$), but the total occupancy

of DNA by Mg^{2+} is smaller than that of Ca^{2+}, which disagrees with the experimental preference.[46] This discrepancy may be due to the lack of direct binding between Mg^{2+} and DNA and/or an overestimation of the Ca^{2+}-phosphate oxygen interaction. Mg^{2+} has a tightly held first solvation shell and does not directly bind to DNA in these simulations. In contrast, Ca^{2+} has a strong interaction with phosphate oxygen atoms and a large portion of Ca^{2+} ions form direct contacts with the phosphate backbone of DNA. As a result, the occupancy of DNA predicted by these simulations is underestimated for Mg^{2+} and overestimated for Ca^{2+}.

For the alkaline earth metal ions studied, the phosphate backbone constitutes the majority of the total occupancy with values from 0.34 to 0.71 (Fig. 5). The major groove is the second largest contributor with values from 0.10 to 0.15. Occupancy of the minor groove is relatively small ($<$ 0.01) as well as simultaneous occupancy of the phosphate backbone and either the major or the minor groove ($\leq$ 0.05). Overall, alkaline earth metal ions preferentially bind to the phosphate backbone and the major groove of dsDNA, where the phosphate backbone is preferred over the major groove.

Because total occupancy varies for each ion, the percentage of bound ions within a specific DNA binding site is used to compare the extent of preferential binding among ions. The percentage of bound Mg^{2+} ions that occupy the phosphate backbone is 67%, which is about twice that of the major groove (30%). For the larger alkaline earth metal ions, the percentage of bound ions that occupy the phosphate backbone decreases as the ionic radius increases: 89%, 75%, and 66% for Ca^{2+}, Sr^{2+}, and Ba^{2+}, respectively. The percentage of bound ions that occupy the major groove is relatively small for Sr^{2+} (16%) and Ba^{2+} (17%) and negligible for Ca^{2+} (3%). Therefore, the alkaline earth metal ions Ca^{2+}, Sr^{2+}, and Ba^{2+} have a stronger preference for the phosphate backbone over the major groove compared to Mg^{2+}.

Sequence-Dependent Binding in Major Groove

Ion counting experiments with dsDNA report sequence-independent results,[46] whereas experimental studies on single-strand DNA indicate that divalent metal ions preferentially bind to cytosine (C) and guanine (G) compared to adenine (A) and thymine (T) nucleotides.[106] These seemingly disparate results can be explained by sequence-dependent ion binding within the major groove of dsDNA, but sequence-independent binding at the phosphate backbone. The simulations presented in this work reproduce these experimental observations. The GC track within the major groove preferentially binds more divalent ions than the AT track, but occupancy of the phosphate backbone is independent of the nucleotide sequence (Fig. S9). These results agree with previous simulations of Mg^{2+} with the same DNA duplex sequence.[56] Interestingly, this sequence-dependent binding within the major groove of dsDNA is observed for all alkaline earth metal ions studied, regardless of ion size, binding motif (direct versus indirect binding), or total occupancy of DNA.

Major Groove Binding at Guanine N7 and O6 Atoms

It is generally accepted that the preferred binding site of divalent metal ions in the major groove is the N7 atom of guanine,[43–45,48,51,107] but some studies suggest that metal ions may also bind to the O6 atom of guanine.[45,51,52,54,55] The RDFs of the alkaline earth metal ions studied here demonstrate binding at both the N7 and O6 sites of guanine (Fig. 4). The heights of the first peaks of the Ba^{2+} and Mg^{2+} RDFs are larger for the O6 atom than that of the N7 atom. In addition, the most probable distance between each ion and the O6 atom of guanine is 0.1-0.3 Å smaller than that of the N7 atom. These observations suggest that alkaline earth metal ions within the major groove of dsDNA are more likely to bind to the O6 atom rather than the N7 atom of guanine.

To make a quantitative comparison, the occupancy of each electronegative atom within the major groove of dsDNA is shown in Fig. 6. For the alkaline earth metal ions studied, the occupancy of the O6 atom of guanine is slightly larger than that of the N7 atom. Additional analysis based on classifying each bound ion by its shortest contact shows that the majority of divalent metal ions bound within the major groove of dsDNA are simultaneously bound to both the N7 and O6 atoms of guanine with a shorter contact to the O6 atom (Fig. S10). The majority of these contacts are indirect contacts, but similar trends are observed for simultaneous direct and indirect binding of Sr^{2+} and Ba^{2+}. Therefore, the alkaline earth metal ions studied likely form simultaneous interactions with both the N7 and O6 atoms of guanine within the major groove of dsDNA, with a small preference for the O6 atom over the N7 atom.
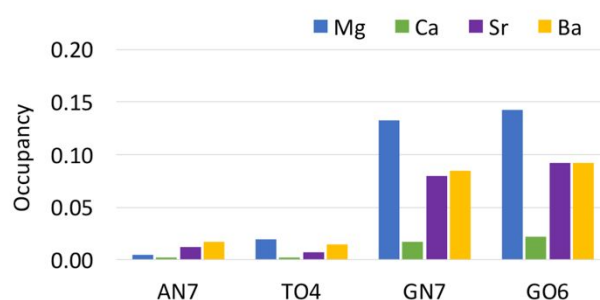

Fig. 6 Occupancy of the N7 atom of adenine (AN7), O4 atom of thymine (TO4), N7 atom of guanine (GN7), and O6 atom of guanine (GO6) within the major groove of dsDNA by alkaline earth metal ions.

Overall Comparison of Alkaline Earth Metal Ions

The RDFs for alkaline earth metal ions (Figs. 2 – 4) reveal that Mg^{2+} has a tightly held first solvation shell that only allows indirect binding to dsDNA, whereas Ca^{2+}, Sr^{2+}, and Ba^{2+} have variable first solvation shells that allow direct and indirect binding. Although RDFs indicate the binding motif present, they do not distinguish among direct binding only, indirect binding only or simultaneous direct and indirect binding. The occupancy of the phosphate backbone and the major groove of dsDNA classified by these types of binding are shown in Fig. 7. The ions with variable first solvation shells (Ca^{2+}, Sr^{2+}, and Ba^{2+}) exhibit opposing trends at the phosphate backbone and major groove of dsDNA.

At the phosphate backbone (Fig. 7a), Ca^{2+}, Sr^{2+}, and Ba^{2+} ions exhibit all three types of binding, where the number of metal ions that form at least one direct contact with the phosphate backbone decreases with increasing ionic radius: $Ca^{2+} > Sr^{2+} > Ba^{2+}$. Within the major groove (Fig. 7b), the majority of bound Ca^{2+}, Sr^{2+}, and Ba^{2+} ions form only indirect contacts, but the small portion that form at least one direct contact increases with increasing ionic radius: $Ca^{2+} < Sr^{2+} < Ba^{2+}$. Therefore, smaller alkaline earth metal ions with a variable first solvation shell prefer to form direct contacts with the phosphate backbone and indirect contacts within the major groove, whereas larger alkaline earth metal ions prefer to form indirect contacts with both the phosphate backbone and the major groove.
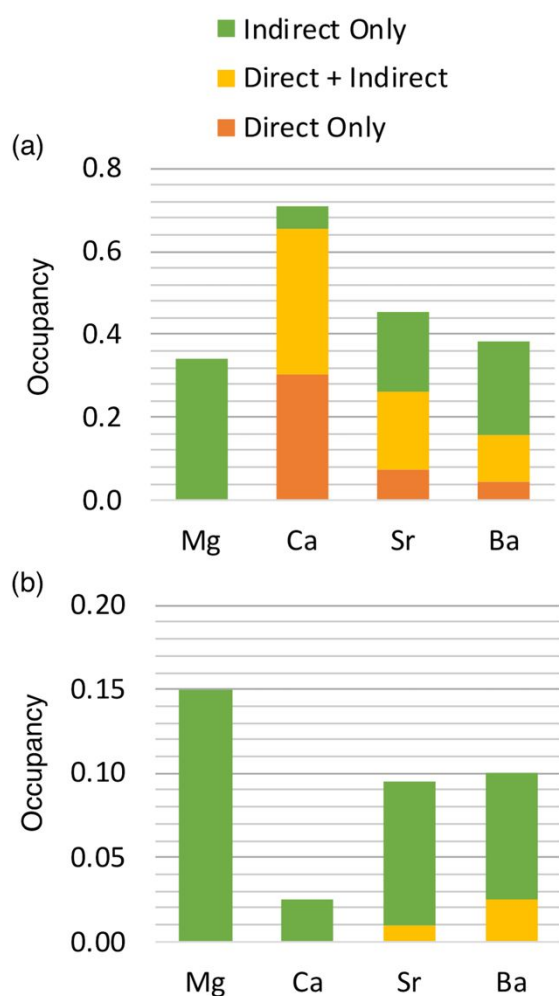

Fig. 7 Occupancy of the (a) phosphate backbone and (b) major groove of dsDNA by alkaline earth metal ions. Bound ions are classified by the type of contact(s): indirect contact(s) only (Indirect Only), simultaneous direct and indirect contacts (Direct + Indirect), or direct contact(s) only (Direct Only).

From a physical perspective, these size-dependent trends may be explained in terms of the strength of the DNA-ion interaction, ion size, and flexibility of the first solvation shell. Due to its smaller ionic radius, the Coulombic attraction between Ca^{2+} and the oxygen atoms of the phosphate backbone is stronger than the Sr^{2+} and Ba^{2+} ions. This stronger attraction

leads to a more favorable interaction between Ca^{2+} ions and the phosphate backbone compared to the larger alkaline earth metal ions. Despite it having a more ordered first solvation shell (Fig. 2), Ca^{2+} is more likely to lose one of its first solvation shell water molecules (Fig. S11) and form a direct contact with the phosphate backbone (Fig. 7). This observation suggests that the energetic stabilization gained by forming a direct contact between Ca^{2+} and phosphate oxygen atom(s) is larger than the energetic penalty of removing a first solvation shell water.

Due to the combined effects of the strong ion-phosphate interaction, ion size, and flexibility of its first solvation shell, Ca^{2+} is more likely to bind to the phosphate backbone and remain there throughout the simulation. Specifically, once a direct contact is formed, Ca^{2+} ions remain directly bound to the phosphate backbone for at least 1 ns, but each ion can bind and unbind for up to 4 binding events. This behavior is evident by fewer binding events (Fig. S12) and long-lived ($>$ 1 ns) residence times (Fig. S13) compared to the other alkaline earth metal ions. Because Ca^{2+} ions strongly bind to the phosphate backbone and remain there for relatively long periods of time, few Ca^{2+} ions are available to travel into and bind to the major groove of dsDNA, resulting in the low occupancy of Ca^{2+} at this binding site (Fig. 7).

As the ionic radius increases, the Coulombic attraction between the alkaline earth metal ions and the phosphate backbone of DNA decreases, resulting in a lower occupancy of the phosphate backbone for Sr^{2+} and Ba^{2+} relative to Ca^{2+} (Fig. 7). Sr^{2+} and Ba^{2+} ions are more likely to retain their first solvation shells (Fig. S11) and form indirect rather than direct contacts with the phosphate backbone (Fig. 7). This result suggests that the energetic penalty of removing a water molecule from the first solvation shell of Sr^{2+} or Ba^{2+} outweighs the energetic stabilization gained by forming a direct contact with the phosphate backbone. As a result, these ions freely bind and unbind to the phosphate backbone throughout the simulation, evident by a larger number of binding events (Fig. S12) and shorter ($<$ 500 ps) residence times (Fig. S13) compared to Ca^{2+} ions. Because Sr^{2+} and Ba^{2+} ions do not bind to the phosphate backbone as strongly as Ca^{2+}, these ions are free to travel into and bind to the major groove of dsDNA, increasing their occupancy of the major groove compared to Ca^{2+} (Fig. 7).

Mg^{2+} does not follow the size-dependent trends observed for Ca^{2+}, Sr^{2+}, and Ba^{2+}. Because Mg^{2+} has the smallest ionic radius of the alkaline earth metal ions, it is expected to have the largest Coulombic attraction to the DNA phosphate backbone and, therefore, have the largest occupancy at this binding site. However, it has a tightly held first solvation shell (Fig. 2) that preferentially forms indirect rather than direct contacts with DNA (Fig. 7). Because Mg^{2+} only forms indirect contacts with DNA, its occupancy of the phosphate backbone is underestimated relative to the larger alkaline earth metal ions. Despite having the lowest occupancy of the phosphate backbone, Mg^{2+} ions are more likely to have intermediate residence times (500 ps – 1 ns) compared to Ca^{2+}, Sr^{2+}, and Ba^{2+} (Fig. S13). Within the major groove, Mg^{2+} follows the trend of increasing indirect binding with decreasing ionic radius, but the occupancy of the major groove by Mg^{2+} is larger than the other

alkaline earth metal ions. This result may be due to long residence times ($>$ 1 ns) within the major groove for Mg^{2+} compared to Ca^{2+}, Sr^{2+}, and Ba^{2+} (Fig. S13). In general, Mg^{2+} does not exhibit the same size-dependent trends observed for the larger alkaline earth metal ions due to its tightly held first solvation shell. An alternative computational approach is necessary to further investigate direct binding of Mg^{2+} to dsDNA, which is observed by experiment.[43,48,51,54]

Comparison of these DNA-ion binding trends provides insight to the competition of alkaline earth metal ions for the DNA ion atmosphere. If present in the same solution, Ca^{2+} is expected to displace the other alkaline earth metal ions near DNA due to its strong preference for forming long-lived direct contacts with the phosphate backbone. Similarly, Sr^{2+} and Ba^{2+} are expected to displace Mg^{2+} at the phosphate backbone due to their potential to form direct contacts with DNA, whereas Mg^{2+} only forms indirect contacts. However, the residence times of Mg^{2+} ions are intermediate in length relative to Sr^{2+} and Ba^{2+}, so Mg^{2+} ions may occupy the phosphate backbone for longer periods of time and prevent Sr^{2+} and Ba^{2+} from binding to DNA. Within the major groove, Mg^{2+} is expected to displace the larger alkaline earth metal ions due to its larger occupancy and longer residence times at this DNA binding site.

Conclusions

This work provides for the first time a direct comparison of DNA-ion binding for a series of alkaline earth metal ions (Mg^{2+}, Ca^{2+}, Sr^{2+}, and Ba^{2+}) using atomistic molecular dynamics simulations. The metal ions were modeled by a force field parameterized to reproduce experimental ion hydration data. This force field is validated for modeling DNA-ion interactions by reproducing experimental ion counting data and ion-phosphate distances. The spatial distribution of the alkaline earth metal ions surrounding a DNA duplex was analyzed using RDFs and occupancy values. Radial distances were used to identify direct and indirect binding and occupancy values provided quantitative comparisons for the number and type of contacts (i.e., direct and indirect) formed between the alkaline earth metal ions and dsDNA. Both RDFs and occupancy values demonstrate that Mg^{2+} ions bind to dsDNA through indirect binding due to its tightly held first solvation shell. In contrast, Ca^{2+}, Sr^{2+}, and Ba^{2+} ions can lose one or more water molecules in their first solvation shell and bind to dsDNA through direct or indirect binding.

The total occupancy of dsDNA decreases in the following order: $Ca^{2+} > Sr^{2+} > Ba^{2+} > Mg^{2+}$. The phosphate backbone is preferred over the major groove and negligible binding occurs in the minor groove. Ca^{2+}, Sr^{2+}, and Ba^{2+} have a stronger preference for the phosphate backbone than Mg^{2+}. DNA-ion binding is independent of the DNA sequence at the phosphate backbone, whereas GC base pairs are preferred within the major groove. Most alkaline earth metal ions bound in the major groove form indirect contacts (i.e., hydrogen bonds) with both the N7 and O6 atoms of guanine simultaneously and have a slight preference for the O6 over the N7 atom. Although there are fewer ions that bind to the major groove compared to the

phosphate backbone, each ion in the major groove typically forms more contacts than the ions bound to the phosphate backbone. These results may provide insight into ion-mediated binding of dsDNA to functionalized surfaces or other nanoscale structures.

The alkaline earth metal ions with flexible first solvation shells (Ca^{2+}, Sr^{2+}, and Ba^{2+}) exhibit size-dependent trends in DNA-ion binding. Ca^{2+} has a strong ion-phosphate interaction that results in long-lived contacts at the phosphate backbone and negligible binding within the major groove. As the ionic radius increases, Sr^{2+} and Ba^{2+} have weaker ion-phosphate interactions and are more likely to form indirect contacts with the phosphate backbone; therefore, these ions can travel into and bind to the major groove. As the smallest alkaline earth metal ion, Mg^{2+} is expected to have the strongest ion-phosphate interaction and thus the largest phosphate backbone occupancy. However, due to its tightly held first solvation shell, the Mg^{2+}-phosphate interaction is shielded relative to the larger alkaline earth metal ions. As a result, Mg^{2+} has intermediate residence times at the phosphate backbone and is free to travel into and bind to the major groove more than the larger alkaline earth metal ions. Overall, alkaline earth metal ions with flexible first solvation shells exhibit size-dependent trends, whereas Mg^{2+} with its tightly held first solvation shell does not.

This work provides a qualitative and quantitative analysis of alkaline earth metal ions binding to dsDNA that accurately reproduces experimental trends. Both the strength of site-specific DNA-ion interactions and metal ion hydration play an important role in determining the preferred DNA binding sites and binding motif (direct or indirect) of alkaline earth metal ions.

Conflicts of Interest

There are no conflicts to declare.

Acknowledgements

References

1   G. C. L. Wong and L. Pollack, Electrostatics of Strongly Charged Biological Polymers: Ion-Mediated Interactions and Self-Organization in Nucleic Acids and Proteins, *Annu. Rev. Phys. Chem.*, 2010, **61**, 171–189.

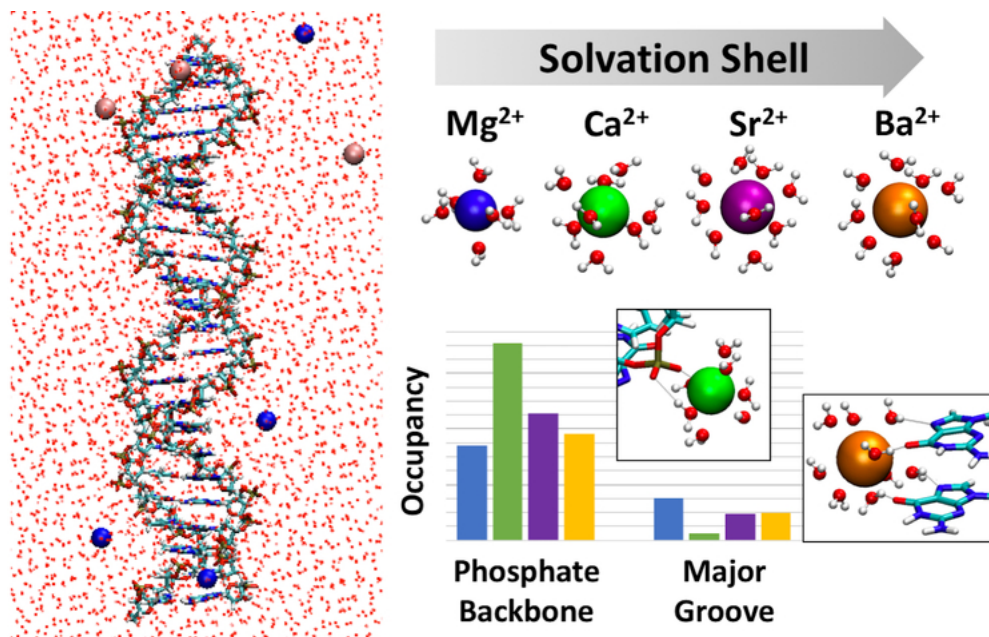2   J. Lipfert, S. Doniach, R. Das and D. Herschlag, Understanding Nucleic Acid–Ion Interactions, *Annu. Rev.*

Biochem., 2014, **83**, 813–841.

3   J. Weston and E. Rappoport, in *Chemistry of Organomagnesium Compounds*, ed. Z. Rappoport, John Wiley & Sons, Ltd, Chichester, UK, 2008, pp. 315–367.

4   N. C. Seeman, DNA in a material world, *Nature*, 2003, **421**, 427–431.

5   O. I. Wilner and I. Willner, Functionalized DNA Nanostructures, *Chem. Rev.*, 2012, **112**, 2528–2556.

6   C.-H. Lu, B. Willner and I. Willner, DNA Nanotechnology: From Sensing and DNA Machines to Drug-Delivery Systems, *ACS Nano*, 2013, **7**, 8320–8332.

7   M. H. Shamsi and H.-B. Kraatz, Interactions of Metal Ions with DNA and Some Applications, *J. Inorg. Organomet. Polym. Mater.*, 2013, **23**, 4–23.

8   A. Samanta and I. L. Medintz, Nanoparticles and DNA – a powerful and growing functional combination in bionanotechnology, *Nanoscale*, 2016, **8**, 9037–9095.

9   Z. Peng and H. Liu, Bottom-up Nanofabrication Using DNA Nanostructures, *Chem. Mater.*, 2016, **28**, 1012–1021.

10 W. Zhou, R. Saran and J. Liu, Metal Sensing by DNA, *Chem. Rev.*, 2017, **117**, 8272–8325.

11 Y. Zhang, J. Tu, D. Wang, H. Zhu, S. K. Maity, X. Qu, B. Bogaert, H. Pei and H. Zhang, Programmable and Multifunctional DNA-Based Materials for Biomedical Applications, *Adv. Mater.*, 2018, **30**, 1703658.

12 H.-Y. Park, S. R. Dugasani, D.-H. Kang, J. Jeon, S. K. Jang, S. Lee, Y. Roh, S. H. Park and J.-H. Park, n- and p-Type Doping Phenomenon by Artificial DNA and M-DNA on Two-Dimensional Transition Metal Dichalcogenides, *ACS Nano*, 2014, **8**, 11603–11613.

13 S. M. Goodman, V. Singh, J. C. Ribot, A. Chatterjee and P. Nagpal, Multiple Energy Exciton Shelves in Quantum-Dot–DNA Nanobioelectronics, *J. Phys. Chem. Lett.*, 2014, **5**, 3909–3913.

14 S. M. Goodman, A. Siu, V. Singh and P. Nagpal, Long-range energy transfer in self-assembled quantum dot-DNA cascades, *Nanoscale*, 2015, **7**, 18435–18440.

15 S. Mutsamwira, E. W. Ainscough, A. C. Partridge, P. J. Derrick and V. V. Filichev, DNA-Based Assemblies for Photochemical Upconversion, *J. Phys. Chem. B*, 2015, **119**, 14045–14052.

16 S. R. Dugasani, B. Paulson, T. Ha, T. S. Jung, B. Gnapareddy, J. A. Kim, T. Kim, H. J. Kim, J. H. Kim, K. Oh and S. H. Park, Fabrication and optoelectronic characterisation of lanthanide- and metal-ion-doped DNA thin films, *J. Phys. D. Appl. Phys.*, 2018, **51**, 285301.

17 S. Dhar, W. L. Daniel, D. A. Giljohann, C. A. Mirkin and S. J. Lippard, Polyvalent Oligonucleotide Gold Nanoparticle Conjugates as Delivery Vehicles for Platinum(IV) Warheads, *J. Am. Chem. Soc.*, 2009, **131**, 14652–14653.

18 I. Turel and J. Kljun, Interactions of Metal Ions with DNA, Its Constituents and Derivatives, which may be Relevant for Anticancer Research, *Curr. Top. Med. Chem.*, 2011, **11**, 2661–2687.

19 S. Vellampatti, G. Chandrasekaran, S. B. Mitta, V.-K. Lakshmanan and S. H. Park, Metallo-Curcumin-Conjugated DNA Complexes Induces Preferential Prostate Cancer Cells Cytotoxicity and Pause Growth of Bacterial Cells, *Sci. Rep.*, 2018, **8**, 14929.

20 Z. Liu, S. H. J. Mei, J. D. Brennan and Y. Li, Assemblage of Signaling DNA Enzymes with Intriguing Metal-Ion Specificities and pH Dependences, *J. Am. Chem. Soc.*, 2003, **125**, 7539–7545.

21 A. A. Gorodetsky, M. C. Buzzeo and J. K. Barton, DNA-Mediated Electrochemistry, *Bioconjug. Chem.*, 2008, **19**, 2285–2296.

22 F. Pu, Z. Huang, J. Ren and X. Qu, DNA/Ligand/Ion-Based Ensemble for Fluorescence Turn on Detection of Cysteine and Histidine with Tunable Dynamic Range, *Anal. Chem.*, 2010, **82**, 8211–8216.

23 Q. Wang, W. Wang, J. Lei, N. Xu, F. Gao and H. Ju, Fluorescence Quenching of Carbon Nitride Nanosheet through Its Interaction with DNA for Versatile Fluorescence Sensing, *Anal. Chem.*, 2013, **85**, 12182–12188.

24 H. Ma and Y. Ma, Solvent effect on electronic absorption, fluorescence, and phosphorescence of acetone in water: revisited by quantum mechanics/molecular mechanics (QM/MM) simulations., *J. Chem. Phys.*, 2013, **138**, 224505.

25 L. Ma, B. Liu, P.-J. J. Huang, X. Zhang and J. Liu, DNA Adsorption by ZnO Nanoparticles near Its Solubility Limit: Implications for DNA Fluorescence Quenching and DNAzyme Activity Assays, *Langmuir*, 2016, **32**, 5672–5680.

26 Q. Zhao, Y. Zhou, Y. Li, W. Gu, Q. Zhang and J. Liu, Luminescent Iridium(III) Complex Labeled DNA for Graphene Oxide-Based Biosensors, *Anal. Chem.*, 2016, **88**, 1892–1899.

27 Y. Meng, P. Liu, W. Zhou, J. Ding and J. Liu, Bioorthogonal DNA Adsorption on Polydopamine Nanoparticles Mediated by Metal Coordination for Highly Robust Sensing in Serum and Living Cells, *ACS Nano*, 2018, **12**, 9070–9080.

28 K. H. Han, J. Y. Kim, S. G. Jo, C. Seo, J. Kim and J. Joo, Sensitive optical bio-sensing of p-type WSe2 hybridized with fluorescent dye attached DNA by doping and de-doping effects, *Nanotechnology*, 2017, **28**, 435501.

29 Y. Fu and J. R. Lakowicz, Enhanced Fluorescence of Cy5-Labeled DNA Tethered to Silver Island Films: Fluorescence Images and Time-Resolved Studies Using Single-Molecule Spectroscopy, *Anal. Chem.*, 2006, **78**, 6238–6245.

30 V. Glembockyte, R. Lincoln and G. Cosa, Cy3 Photoprotection Mediated by Ni^{2+} for Extended Single-Molecule Imaging: Old Tricks for New Techniques, *J. Am. Chem. Soc.*, 2015, **137**, 1116–1122.

31 H. Ohtaki and T. Radnai, Structure and dynamics of hydrated ions, *Chem. Rev.*, 1993, **93**, 1157–1204.

32 Y. Inada, H. Hayashi, K. Sugimoto and S. Funahashi, Solvation Structures of Manganese(II), Iron(II), Cobalt(II), Nickel(II), Copper(II), Zinc(II), and Gallium(III) Ions in Methanol, Ethanol, Dimethyl Sulfoxide, and Trimethyl Phosphate As Studied by EXAFS and Electronic Spectroscopies, *J. Phys. Chem. A*, 1999, **103**, 1401–1406.

33 S. Ramos, G. W. Neilson, A. C. Barnes and M. J. Capitán, Anomalous x-ray diffraction studies of Sr^{2+} hydration in aqueous solution, *J. Chem. Phys.*, 2003, **118**, 5542–5546.

34 P. D'Angelo, V. Migliorati, F. Sessa, G. Mancini and I.

Persson, XANES Reveals the Flexible Nature of Hydrated Strontium in Aqueous Solution, *J. Phys. Chem. B*, 2016, **120**, 4114–4124.

35   M. F. Bush, R. J. Saykally and E. R. Williams, Infrared Action Spectra of $Ca^{2+}(H_2O)_{11-69}$ Exhibit Spectral Signatures for Condensed-Phase Structures with Increasing Cluster Size, *J. Am. Chem. Soc.*, 2008, **130**, 15482–15489.

36   M. F. Bush, J. T. O'Brien, J. S. Prell, C.-C. Wu, R. J. Saykally and E. R. Williams, Hydration of Alkaline Earth Metal Dications: Effects of Metal Ion Size Determined Using Infrared Action Spectroscopy, *J. Am. Chem. Soc.*, 2009, **131**, 13270–13277.

37   F. Jalilehvand, D. Spångberg, P. Lindqvist-Reis, K. Hermansson, I. Persson and M. Sandström, Hydration of the Calcium Ion. An EXAFS, Large-Angle X-ray Scattering, and Molecular Dynamics Simulation Study, *J. Am. Chem. Soc.*, 2001, **123**, 431–441.

38   P. R. Smirnov and V. N. Trostin, Structural parameters of close surroundings of Sr^{2+} and Ba^{2+} ions in aqueous solutions of their salts, *Russ. J. Gen. Chem.*, 2011, **81**, 282–289.

39   J. Neely and R. Connick, Rate of water exchange from hydrated magnesium ion, *J. Am. Chem. Soc.*, 1970, **92**, 3476–3478.

40   K. M. Callahan, N. N. Casillas-Ituarte, M. Roeselová, H. C. Allen and D. J. Tobias, Solvation of Magnesium Dication: Molecular Dynamics Simulation and Vibrational Spectroscopic Study of Magnesium Chloride in Aqueous Solutions, *J. Phys. Chem. A*, 2010, **114**, 5141–5148.

41   L. Helm and A. E. Merbach, Inorganic and Bioinorganic Solvent Exchange Mechanisms, *Chem. Rev.*, 2005, **105**, 1923–1959.

42   I. Morfin, F. Horkay, P. J. Basser, F. Bley, A.-M. Hecht, C. Rochas and E. Geissler, Adsorption of divalent cations on DNA., *Biophys. J.*, 2004, **87**, 2897–2904.

43   M. Langlais, H. A. Tajmir-Riahi and R. Savoie, Raman spectroscopic study of the effects of Ca^{2+}, Mg^{2+}, Zn^{2+}, and Cd^{2+} ions on calf thymus DNA: Binding sites and conformational changes, *Biopolymers*, 1990, **30**, 743–752.

44   J. G. Duguid, V. A. Bloomfield, J. M. Benevides and G. J. Thomas, Raman spectroscopy of DNA-metal complexes. II. The thermal denaturation of DNA in the presence of Sr^{2+}, Ba^{2+}, Mg^{2+}, Ca^{2+}, Mn^{2+}, Co^{2+}, Ni^{2+}, and Cd^{2+}., *Biophys. J.*, 1995, **69**, 2623–2641.

45   V. Andrushchenko and P. Bouř, Infrared Absorption Detection of Metal Ion-Deoxyguanosine Monophosphate Binding: Experimental and Theoretical Study, *J. Phys. Chem. B*, 2009, **113**, 283–291.

46   Y. Bai, M. Greenfeld, K. J. Travers, V. B. Chu, J. Lipfert, S. Doniach and D. Herschlag, Quantitative and Comprehensive Decomposition of the Ion Atmosphere around Nucleic Acids, *J. Am. Chem. Soc.*, 2007, **129**, 14981–14988.

47   A. Z. Li, H. Huang, X. Re, L. J. Qi and K. A. Marx, A gel electrophoresis study of the competitive effects of monovalent counterion on the extent of divalent counterions binding to DNA., *Biophys. J.*, 1998, **74**, 964–

973.

48   J. A. Subirana and M. Soler-López, Cations as Hydrogen Bond Donors: A View of Electrostatic Interactions in DNA, *Annu. Rev. Biophys. Biomol. Struct.*, 2003, **32**, 27–45.

49   G. L. Eichhorn and Y. A. Shin, Interaction of metal ions with polynucleotides and related compounds. XII. The relative effect of various metal ions on DNA helicity, *J. Am. Chem. Soc.*, 1968, **90**, 7323–7328.

50   J. Duguid, V. A. Bloomfield, J. Benevides and G. J. Thomas, Raman spectroscopy of DNA-metal complexes. I. Interactions and conformational effects of the divalent cations: Mg, Ca, Sr, Ba, Mn, Co, Ni, Cu, Pd, and Cd., *Biophys. J.*, 1993, **65**, 1916–1928.

51   R. Ahmad, H. Arakawa and H. A. Tajmir-Riahi, A comparative study of DNA complexation with Mg(II) and Ca(II) in aqueous solution: major and minor grooves bindings., *Biophys. J.*, 2003, **84**, 2460–2466.

52   X. Shui, L. McFail-Isom, G. G. Hu and L. D. Williams, The B-DNA dodecamer at high resolution reveals a spine of water on sodium., *Biochemistry*, 1998, **37**, 8341–8355.

53   V. A. Buckin, B. I. Kankiya, D. Rentzeperis and L. A. Marky, Mg^{2+} recognizes the sequence of DNA through its hydration shell, *J. Am. Chem. Soc.*, 1994, **116**, 9423–9429.

54   F. Leonarski, L. D'Ascenzo and P. Auffinger, Binding of metals to purine N7 nitrogen atoms and implications for nucleic acids: A CSD survey, *Inorganica Chim. Acta*, 2016, **452**, 82–89.

55   B. Lippert, Multiplicity of metal ion binding patterns to nucleobases, *Coord. Chem. Rev.*, 2000, **200–202**, 487–516.

56   W. Li, L. Nordenskiöld and Y. Mu, Sequence-specific Mg^{2+}-DNA interactions: a molecular dynamics simulation study., *J. Phys. Chem. B*, 2011, **115**, 14713–14720.

57   J. Yoo and A. Aksimentiev, Competitive binding of cations to duplex DNA revealed through molecular dynamics simulations., *J. Phys. Chem. B*, 2012, **116**, 12946–54.

58   S. Mukherjee and D. Bhattacharyya, Influence of divalent magnesium ion on DNA: molecular dynamics simulation studies, *J. Biomol. Struct. Dyn.*, 2013, **31**, 896–912.

59   T. J. Robbins and Y. Wang, Effect of initial ion positions on the interactions of monovalent and divalent ions with a DNA duplex as revealed with atomistic molecular dynamics simulations, *J. Biomol. Struct. Dyn.*, 2013, **31**, 1311–1323.

60   T. J. Robbins, J. D. Ziebarth and Y. Wang, Comparison of monovalent and divalent ion distributions around a DNA duplex with molecular dynamics simulation and a Poisson-Boltzmann approach., *Biopolymers*, 2014, **101**, 834–848.

61   O. Allnér, L. Nilsson and A. Villa, Magnesium Ion–Water Coordination and Exchange in Biomolecular Simulations, *J. Chem. Theory Comput.*, 2012, **8**, 1493–1502.

62   J. Åqvist, Ion-water interaction potentials derived from free energy perturbation simulations, *J. Phys. Chem.*, 1990, **94**, 8021–8024.

63   I. S. Joung and T. E. Cheatham, Determination of Alkali and Halide Monovalent Ion Parameters for Use in Explicitly Solvated Biomolecular Simulations, *J. Phys. Chem. B*, 2008, **112**, 9020–9041.

64   J. Yoo and A. Aksimentiev, Improved Parametrization of Li^+,

Na$^+$, K$^+$, and Mg^{2+} Ions for All-Atom Molecular Dynamics Simulations of Nucleic Acid Systems, *J. Phys. Chem. Lett.*, 2012, **3**, 45–50.

65 F. Duarte, P. Bauer, A. Barrozo, B. A. Amrein, M. Purg, J. Aqvist and S. C. L. Kamerlin, Force field independent metal parameters using a nonbonded dummy model., *J. Phys. Chem. B*, 2014, **118**, 4351–4362.

66 A. Savelyev and A. D. MacKerell, Balancing the interactions of ions, water, and DNA in the Drude polarizable force field., *J. Phys. Chem. B*, 2014, **118**, 6742–57.

67 A. Savelyev and A. D. MacKerell, Competition among Li(+), Na(+), K(+), and Rb(+) monovalent ions for DNA in molecular dynamics simulations using the additive CHARMM36 and Drude polarizable force fields., *J. Phys. Chem. B*, 2015, **119**, 4428–4440.

68 M. Kumar, T. Simonson, G. Ohanessian and C. Clavaguéra, Structure and Thermodynamics of Mg:Phosphate Interactions in Water: A Simulation Study, *ChemPhysChem*, 2015, **16**, 658–665.

69 N. Sundaresan, C. K. S. Pillai and C. H. Suresh, Role of Mg^{2+} and Ca^{2+} in DNA bending: evidence from an ONIOM-based QM-MM study of a DNA fragment., *J. Phys. Chem. A*, 2006, **110**, 8826–31.

70 N. Sundaresan, C. H. Suresh, T. Thomas, T. J. Thomas and C. K. S. Pillai, Liquid Crystalline Phase Behavior of High Molecular Weight DNA: A Comparative Study of the Influence of Metal Ions of Different Size, Charge and Binding Mode, *Biomacromolecules*, 2008, **9**, 1860–1869.

71 G. S. Freeman, D. M. Hinckley and J. J. de Pablo, A coarse-grain three-site-per-nucleotide model for DNA with explicit ions, *J. Chem. Phys.*, 2011, **135**, 165104.

72 J. Yoo, J. Wilson and A. Aksimentiev, Improved model of hydrated calcium ion for molecular dynamics simulations using classical biomolecular force fields, *Biopolymers*, 2016, **105**, 752–763.

73 P. Li and K. M. Merz, Taking into Account the Ion-Induced Dipole Interaction in the Nonbonded Model of Ions, *J. Chem. Theory Comput.*, 2014, **10**, 289–297.

74 J. Šponer, J. V. Burda, M. Sabat, J. Leszczynski and P. Hobza, Interaction between the Guanine−Cytosine Watson−Crick DNA Base Pair and Hydrated Group IIa (Mg^{2+}, Ca^{2+}, Sr^{2+}, Ba^{2+}) and Group IIb (Zn^{2+}, Cd^{2+}, Hg^{2+}) Metal Cations, *J. Phys. Chem. A*, 1998, **102**, 5951–5957.

75 J. Šponer, M. Sabat, J. V. Burda, J. Leszczynski and P. Hobza, Interaction of the Adenine−Thymine Watson−Crick and Adenine−Adenine Reverse-Hoogsteen DNA Base Pairs with Hydrated Group IIa (Mg^{2+}, Ca^{2+}, Sr^{2+}, Ba^{2+}) and IIb (Zn^{2+}, Cd^{2+}, Hg^{2+}) Metal Cations: Absence of the Base Pair Stabilization by Metal-I, *J. Phys. Chem. B*, 1999, **103**, 2528–2534.

76 J. Muñoz, J. Sponer, P. Hobza, M. Orozco and F. J. Luque, Interactions of Hydrated Mg^{2+} Cation with Bases, Base Pairs, and Nucleotides. Electron Topology, Natural Bond Orbital, Electrostatic, and Vibrational Study, *J. Phys. Chem. B*, 2001, **105**, 6051–6060.

77 A. S. Petrov, G. Lamm and G. R. Pack, Water-Mediated Magnesium-Guanine Interactions, *J. Phys. Chem. B*, 2002,

106, 3294–3300.

78 L. Rulíšek and J. Šponer, Outer-Shell and Inner-Shell Coordination of Phosphate Group to Hydrated Metal Ions (Mg^{2+}, Cu^{2+}, Zn^{2+}, Cd^{2+}) in the Presence and Absence of Nucleobase. The Role of Nonelectrostatic Effects, *J. Phys. Chem. B*, 2003, **107**, 1913–1923.

79 A. S. Petrov, G. R. Pack and G. Lamm, Calculations of Magnesium−Nucleic Acid Site Binding in Solution, *J. Phys. Chem. B*, 2004, **108**, 6072–6081.

80 A. S. Petrov, J. Funseth-Smotzer and G. R. Pack, Computational study of dimethyl phosphate anion and its complexes with water, magnesium, and calcium, *Int. J. Quantum Chem.*, 2005, **102**, 645–655.

81 I. Solt, I. Simon, A. G. Császár and M. Fuxreiter, Electrostatic versus nonelectrostatic effects in DNA sequence discrimination by divalent ions Mg^{2+} and Mn^{2+}., *J. Phys. Chem. B*, 2007, **111**, 6272–6279.

82 Y. Zhang and K. Huang, On the interactions of hydrated metal cations (Mg^{2+}, Mn^{2+}, Ni^{2+}, Zn^{2+}) with guanine−cytosine Watson−Crick and guanine−guanine reverse-Hoogsteen DNA base pairs, *J. Mol. Struct. THEOCHEM*, 2007, **812**, 51–62.

83 R. Oliva and L. Cavallo, Frequency and Effect of the Binding of Mg^{2+}, Mn^{2+}, and Co^{2+} Ions on the Guanine Base in Watson−Crick and Reverse Watson−Crick Base Pairs, *J. Phys. Chem. B*, 2009, **113**, 15670–15678.

84 P. Li, B. P. Roberts, D. K. Chakravorty and K. M. Merz, Rational Design of Particle Mesh Ewald Compatible Lennard-Jones Parameters for +2 Metal Cations in Explicit Solvent., *J. Chem. Theory Comput.*, 2013, **9**, 2733–2748.

85 M. J. Abraham, T. Murtola, R. Schulz, S. Páll, J. C. Smith, B. Hess and E. Lindahl, GROMACS: High performance molecular simulations through multi-level parallelism from laptops to supercomputers, *SoftwareX*, 2015, **1–2**, 19–25.

86 W. L. Jorgensen, J. Chandrasekhar, J. D. Madura, R. W. Impey and M. L. Klein, Comparison of simple potential functions for simulating liquid water, *J. Chem. Phys.*, 1983, **79**, 926.

87 V. Hornak, R. Abel, A. Okur, B. Strockbine, A. Roitberg and C. Simmerling, Comparison of multiple Amber force fields and development of improved protein backbone parameters, *Proteins Struct. Funct. Bioinforma.*, 2006, **65**, 712–725.

88 A. Pérez, I. Marchán, D. Svozil, J. Sponer, T. E. Cheatham, C. A. Laughton and M. Orozco, Refinement of the AMBER force field for nucleic acids: improving the description of alpha/gamma conformers., *Biophys. J.*, 2007, **92**, 3817–3829.

89 M. Zgarbová, J. Šponer, M. Otyepka, T. E. Cheatham, R. Galindo-Murillo and P. Jurečka, Refinement of the Sugar-Phosphate Backbone Torsion Beta for AMBER Force Fields Improves the Description of Z- and B-DNA, *J. Chem. Theory Comput.*, 2015, **11**, 5723–5736.

90 I. Ivani, P. D. Dans, A. Noy, A. Pérez, I. Faustino, A. Hospital, J. Walther, P. Andrio, R. Goñi, A. Balaceanu, G. Portella, F. Battistini, J. L. Gelpí, C. González, M. Vendruscolo, C. A. Laughton, S. A. Harris, D. A. Case and M. Orozco, Parmbsc1:

A refined force field for DNA simulations, *Nat. Methods*, 2015, **13**, 55–58.

91   P. D. Dans, I. Ivani, A. Hospital, G. Portella, C. González and M. Orozco, How accurate are accurate force-fields for B-DNA?, *Nucleic Acids Res.*, 2017, **45**, 4217-4230.

92   U. Essmann, L. Perera, M. L. Berkowitz, T. Darden, H. Lee and L. G. Pedersen, A smooth particle mesh Ewald method, *J. Chem. Phys.*, 1995, **103**, 8577–8593.

93   G. Bussi, D. Donadio and M. Parrinello, Canonical sampling through velocity rescaling, *J. Chem. Phys.*, 2007, **126**, 014101.

94   M. Parrinello and A. Rahman, Polymorphic transitions in single crystals: A new molecular dynamics method, *J. Appl. Phys.*, 1981, **52**, 7182–7190.

95   S. Miyamoto and P. A. Kollman, Settle: An analytical version of the SHAKE and RATTLE algorithm for rigid water models, *J. Comput. Chem.*, 1992, **13**, 952–962.

96   B. Hess, P-LINCS: A Parallel Linear Constraint Solver for Molecular Simulation, *J. Chem. Theory Comput.*, 2008, **4**, 116–122.

97   M. Pasi, J. H. Maddocks and R. Lavery, Analyzing ion distributions around DNA: sequence-dependence of potassium ion distributions from microsecond molecular dynamics, *Nucleic Acids Res.*, 2015, **43**, 2412–2423.

98   S. A. Pabit, S. P. Meisburger, L. Li, J. M. Blose, C. D. Jones and L. Pollack, Counting Ions around DNA with Anomalous Small-Angle X-ray Scattering, *J. Am. Chem. Soc.*, 2010, **132**, 16334–16336.

99   R. Das, T. T. Mills, L. W. Kwok, G. S. Maskel, I. S. Millett, S. Doniach, K. D. Finkelstein, D. Herschlag and L. Pollack, Counterion Distribution around DNA Probed by Solution X-Ray Scattering, *Phys. Rev. Lett.*, 2003, **90**, 188103.

100   K. Andresen, R. Das, H. Y. Park, H. Smith, L. W. Kwok, J. S. Lamb, E. J. Kirkland, D. Herschlag, K. D. Finkelstein and L. Pollack, Spatial Distribution of Competing Ions around DNA in Solution, *Phys. Rev. Lett.*, 2004, **93**, 248103.

101   R. Caminiti, Complex formation and phosphate-H_2O interactions in a concentrated aqueous $Mg(H_2PO_4)_2$ solution., *J. Mol. Liq.*, 1984, **28**, 191–204.

102   P. Satpati, C. Clavaguéra, G. Ohanessian and T. Simonson, Free Energy Simulations of a GTPase: GTP and GDP Binding to Archaeal Initiation Factor 2, *J. Phys. Chem. B*, 2011, **115**, 6749–6763.

103   T. Simonson and P. Satpati, Simulating GTP:Mg and GDP:Mg with a simple force field: A structural and thermodynamic analysis, *J. Comput. Chem.*, 2013, **34**, 836–846.

104   J. Melcr, H. Martinez-Seara, R. Nencini, J. Kolafa, P. Jungwirth and O. H. S. Ollila, Accurate Binding of Sodium and Calcium to a POPC Bilayer by Effective Inclusion of Electronic Polarization, *J. Phys. Chem. B*, 2018, **122**, 4546–4557.

105   G. Chillemi, P. D'Angelo, N. V. Pavel, N. Sanna and V. Barone, Development and Validation of an Integrated Computational Approach for the Study of Ionic Species in Solution by Means of Effective Two-Body Potentials. The Case of Zn^{2+}, Ni^{2+}, and Co^{2+} in Aqueous Solutions, *J. Am.*

Chem. Soc., 2002, **124**, 1968–1976.

106   J. G. Holland, J. N. Malin, D. S. Jordan, E. Morales and F. M. Geiger, Specific and nonspecific metal ion-nucleotide interactions at aqueous/solid interfaces functionalized with adenine, thymine, guanine, and cytosine oligomers., *J. Am. Chem. Soc.*, 2011, **133**, 2567–2570.

107   E. Moldrheim, B. Andersen, N. Å. Frøystein and E. Sletten, Interaction of manganese(II), cobalt(II) and nickel(II) with DNA oligomers studied by 1H NMR spectroscopy, *Inorganica Chim. Acta*, 1998, **273**, 41–46.

Classical molecular dynamics simulations reveal size-dependent trends of alkaline earth metal ions binding to DNA are due to ion size and hydration behavior.

63x39mm (300 x 300 DPI)